Antenna-Coupled Vacuum Channel Nano-diode with High Quantum Efficiency

Received 00th January 20xx,
Accepted 00th January 20xx

Shenghan Zhou, [a,b] Ke Chen, [a,b] Xiangdong Guo , [a,b] Matthew Thomas Cole, [a,b] Yu Wu, [c] Zhenjun Li, [a,b] Shunping Zhang, [c] Chi Li *[a,b]† and Qing Dai *[a,b]††

Vacuum channel diode can serve as a platform for converting free-space electromagnetic radiation into electronic signals within an ultrafast timescale. However, the conversion efficiency is typically very low because conventional vacuum channel diode suffers from high surface barriers, especially when using lower energy photon excitation (near-infrared photons or lower). Here, we report on an optical antenna-coupled vacuum channel nano-diode, with a greatly improved quantum efficiency up to ~ 4% at 800 nm excitation, an efficiency several orders of magnitude higher than any previously reported value. The nano diodes are formed at the cleaved edge of a metal-insulator-semiconductor (MIS) structure, where a gold thin film with nanohole array serves as both metal electrode and light-harvesting antenna. At the nanoholes-insulator interface, the tunneling barrier is greatly reduced due to the Coulombic repulsion induced high local electron density, that the resonant plasmons induced hot electron population can readily inject into the vacuum channel. The presented vertical tertiary MIS junction enables a new class of high-efficiency, polarization-specific and wavelength- sensitive optical modulated photodetector that has the potential for developing opto-electronic systems.

Introduction

Due to the ballistic electrons transport behavior, vacuum devices support higher operation speeds and higher data transmission bandwidths than conventional electronic devices in addition to high power transmission. For interelectrode gaps of less than 100 nm, integration challenges associated with the need for, and formation of ultra-high vacuum are removed, with effective transport through such gaps occurring even in air. With the emergence of ultra-precise nanoscale manufacturing, vacuum electronics are becoming increasingly feasible as a means of developing low-energy consumption, high-speed integrated optoelectronic devices.

Optical antennas can efficiently couple free-space light into nanoscale volumes or vice verse. Such light-focusing properties are mediated by the formation of surface plasmons, a collective oscillation of free electrons with respect to the ion background. Integrating solid-state devices and metallic optical antenna have been widely employed in energy harvesting,[1-4] imaging,[5-7] and a wide range of light detection technologies.[8-10] Optical antennas have also been coupled into nanoscale vacuum devices, [11, 12] which may display great advantage in ultrafast light information processing. However, strong-field laser (around 10^{12} W/cm^2 in the infrared range) is required to drive the electrons out of the high vacuum barrier (work function 4~5 eV), which is in multiphoton and strong field regime.[11]

Here, we report on a highly-efficient optically modulated vacuum channel nano-diode array that operates in the weak light regime. A greatly enhanced quantum efficiency of ~ 4% is obtained at 800 nm excitation. This is achieved by exploiting a greatly reduced interfacial vacuum barrier at the edge of a metal–insulator–semiconductor (MIS) capacitor structure. The present research have a great potential in ultrafast light information processing devices, such as plasmon enhanced photodetector, surface plasmon logic circuit, etc.

Results and Discussion

Device fabrication and operation principle

Figure 1a schematically depicts the fabricated MIS structure. The vacuum channel nano-diodes were fabricated by spatially selective focused-ion-beam etching (FIB). The MIS structure consists of a 60-nm-thick Au layer, 30-nm-thick SiO_2 layer, on an n-type Si substrate (phosphorus-doped, 0.003 Ω cm, (100), 500±10 μm). The active optical antenna coupled vacuum channel nano-diode consists of an array of independent, rectangular nanoholes etched into the n-Si substrate. Figure 1b shows a scanning electron microscope (SEM) image of a

[a.] Division of Nanophotonics, CAS Center for Excellence in Nanoscience, National Center for Nanoscience and Technology, Beijing 100190, P. R. China.
[b.] Center of Materials Science and Optoelectronics Engineering, University of Chinese Academy of Sciences, Beijing 100049, P. R. China.
[c.] School of Physics and Technology, Wuhan University, Wuhan 430072, China.
† E-mail: lichi@nanoctr.cn
†† E-mail: daiq@nanoctr.cn
Electronic Supplementary Information (ESI) available: [details of any supplementary information available should be included here]. See DOI: 10.1039/x0xx00000x

representative fabricated device. A typical hole size is 500 (±12) nm × 100 (±18) nm. The distance between two adjacent holes is around 500 nm. Two perpendicular symmetry planes in the rectangular nanoholes support both longitudinal and transverse plasmon resonances, with the frequency of these resonances determined by the nanoholes' designed geometry.

The MIS capacitor structures support the formation of an interfacial quasi-two dimensional electron gas (2DEG).[13, 14] At the 2DEG edge, strong Coulombic repulsion occurs which significantly reduces the effective vacuum barrier height.[15-18] In this diode structure, the channel length is determined by the controlled thickness of the insulator layer between the anode and the cathode. The insulator thickness (30 nm) was smaller than the mean free path of air (~69 nm) in order to allow for in-air operation of the device. Therefore, the low-emission-barrier vacuum channel nano-diodes are formed at the edge the nanoholes, as shown in Figure 1c. Figure 1d shows the energy band diagram during negative bias. Compared with the inside (dotted line), the vacuum barrier is greatly reduced at the edge of the MIS structure (red line). Therefore, under laser irradiation on the top electrode, electrons subsequently tunneling through the barrier more easily following the absorption of energy photons.

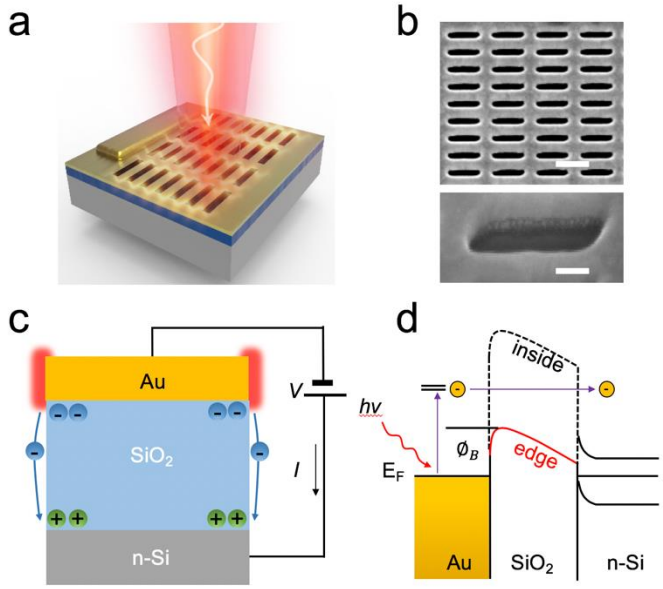

Figure 1. The antenna coupled vacuum channel nanoscale diode. (a) Schematic depiction of the vacuum channel nano-diode fabricated by FIB etching consist of an array of rectangular nanoholes operating during laser induced plasmon resonance at the edge of MIS structure. (b) The top is scanning electron micrograph of a representative fabricated device (6 × 15 array with 500 nm × 100 nm, Scale bar: 1 μm). The bottom is an edge of a nanohole at higher magnification (Scale bar: 500 nm, tilt angle = 45°). (c) Schematic of the electron emission and transport in nano vacuum channels: Au electrode under negatively bias. Note the electron emission from the edge of 2DEG is from gold to silicon. (d) Energy band diagram with the Au electrode during negative bias. The dotted line indicates the energy band of the inside of MIS structure. Where $\emptyset_B$ is the barrier height, and E_f are Fermi level. During laser irradiation on the top electrode, electrons are excited to a higher energy level by gaining the energy of a photon and then tunneling through the barrier. The barrier height at the edge of MIS structure is greatly reduced than the inside.

Transport characteristics

The electrical properties of a representative set of 90 vacuum channel nano-diodes were measured (Keithley Model 4200-SCS). When applying a negative bias on the Au electrode with the Si grounded, the diodes revealed a typical negative biased characteristic; with electron emission in the Au-to-Si direction (Figure 1c). The emission behavior of patterned and unpatterned MIS structures was explored. Figure 2a shows typical static current-versus-voltage (I-V) curves of both patterned and unpatterned devices, in the dark, under different negative bias. A 300 pA (-1V) leakage current (black line, Figure 2a) was measured prior to FIB etching, which is significantly less than the tunneling current (60 nA at -1 V, red line, Figure 2a) measured following device fabrication, suggesting morphological dependent enhancement in the emission current.

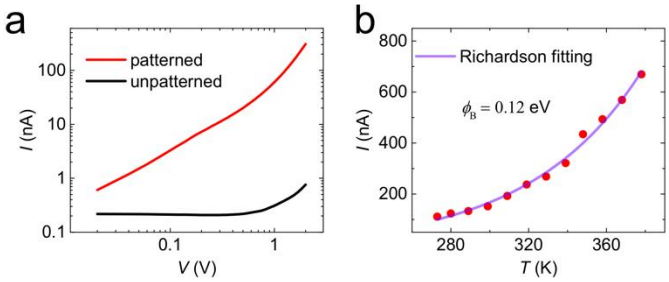

Figure 2. Electron transport in the vacuum channel nanoscale diode. (a) Measured *I-V* characteristics of vacuum channel nano-diode under negatively bias. (b) The current curve of the representative device versus temperature (Au electrode biased to -2 V). The barrier height is 0.12 eV calculated by Richardson fitting.

The barrier height has also been explored through temperature-dependent transport studies. As the vacuum barrier is greatly reduced at the edge of the MIS structure, the electron emission becomes particularly temperature sensitive. We measured the temperature-dependent electron emission properties of the representative devices, which is shown in Figure 2b. According to thermionic emission theory, the height of vacuum barrier can be estimated by Richardson formula,

$$I = \boldsymbol{I_0}(\mathbf{e}^{\boldsymbol{qV/kT}} - \mathbf{1}) \quad (1)$$

Where I is the emission current, $\boldsymbol{I_0}$ is the emission current at zero bias voltage, $\boldsymbol{I_0} = \mathbf{AK}\boldsymbol{T}^{\mathbf{2}}\mathbf{e}^{-\boldsymbol{q\emptyset_B/kT}}$, $\boldsymbol{V}$ is the applied bias voltage, $\mathbf{A}$ is the device emission area, $\boldsymbol{\emptyset_B}$ is the barrier height, $\boldsymbol{T}$ is the temperature, $\mathbf{K} \approx 100$ A/ (cm^2/K^2) is Richardson constant and the $\boldsymbol{k}$ is Boltzmann constant. When the top electrode is negatively biased (-2 V), the vacuum barrier height at the edge of the MIS structure is of the order of ~0.12 eV, which is much lower than 0.5 eV[10] and 2.6 eV[19] previous reported for similar devices.

Photo response

Having demonstrated the occurrence of low-barrier electron emission at the MIS edges, we now investigate the photo response of the device. We aim to realize an enhanced photo response on the patterned MIS structure; in so far as demonstrating that the energetic electrons excited by the plasmon resonance can transport readily tunneling through the greatly reduced vacuum barrier.

90 vacuum channel nano-diodes were tested under illumination (λ =800 ± 6 nm) from a picosecond (τ = 100 ps) ultrafast laser (Wuhan YSL Photonics, SC-Pro7). Optical excitation was focused on the sample using a 10× microscope objective to produce a 10 μm diameter spot size. Here we demonstrate that the photocurrent generation results from hot electron emission and

that such emission can be dramatically enhanced by driving a surface plasmon resonance in the Au electrode. Initially hot electrons are generated in the Au contact due to photon absorption. The generated hot electrons are readily injected into the oxide due to the reduced barrier. The injected electrons across the oxide and contribute to the measured photocurrent. Figure 3 shows the photo response characteristics of the vacuum channel nano-diodes. The photocurrent obtained from our devices is determined directly by the geometric properties of the etched nanohole-based antenna. The polarization dependence of the photocurrent also follows that of the geometrically asymmetric nanoholes which afford a highly polarization dependent response (red points, Figure 3a). The polarization response profiles follow a $\cos^2(\theta)$ angular dependence, characteristic of an ideal dipole antenna (purple line, Figure 3a), suggesting the dipole-mode emission are caused by plasmon resonance from the MIS junctions. Deviations between the simulation and measured polarization curves are due to non-idealities in the nanohole geometries, including edge roughness, which has the net effect of smearing subtle additional spectral resonances within the structures response. For light polarized along the long (transverse) axis, we observe >90% attenuation of the photocurrent with respect to the longitudinal polarization.

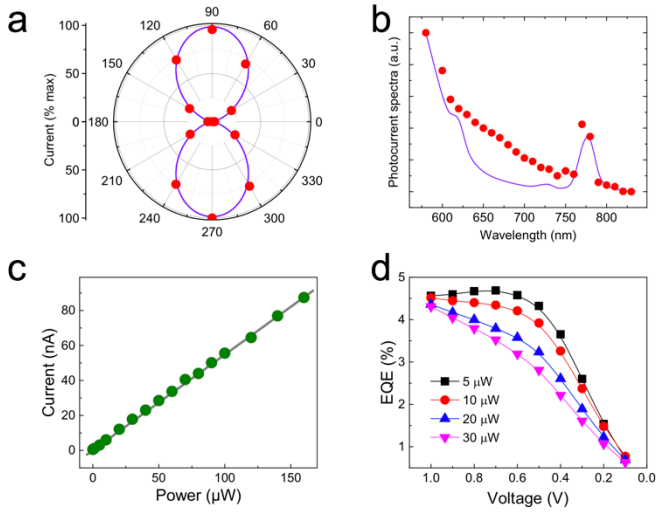

Figure 3. Photo response characteristics of the vacuum channel nanoscale diode. (a) Photocurrent polarization dependence during device excitation at λ=633 nm (red points), exhibiting a $\cos^2(\theta)$ angular dependence (purple line). (b) Theoretically calculated absorption spectra (purple line) and experimentally measured photocurrent spectra (red points) of the device at polarizer angle 0° (parallel to the long axis). (c) Photocurrent for the representative device as a function of input laser power (Au electrode biased to -1 V). (d) Plot of the measured external quantum efficiency (EQE) as a function of applied voltage for different input laser power.

The spectral response directly follows the transverse dipole absorption resonance of the plasmon mode excited on the structure. Responsivity curves of the device are shown in Figure 3b. Significant agreement between experimental photocurrent spectra (red points, Figure 3b) as a function of antenna resonant frequency and optical absorption spectra calculated using theoretical methods (purple line, Figure 3b) is noted. As shown in Figure 3b, when the laser polarization is 0° (parallel to the long axis), the measured photocurrent spectrum has a peak near 780 nm, consistent with the peak position of the simulated plasmon resonance. When photocurrent measurements are performed on multiple antenna arrays, each with a different resonant frequency, it is envisaged that such devices may function as an aggressively miniaturized single-chip spectrometer. This spectroscopic functionality is due to the relationship between photocurrent amplitude and the amplitude of the plasmon resonance at a given frequency and this spectral sensitivity can be used to determine the wavelength of the incident light.

The change in illumination optical power at a single wavelength (λ =800 nm) results in a linear response with photocurrent. The photocurrent is developed from a single incident photon to a single hot electron within this range of incident light intensities.[20-24] The corresponding I-P curve is shown in Figure 3c, significant linearity is noted, which supports our claim of linearity in the photocurrent generation process with absorbed light power.

The overall quantum efficiency of the vacuum channel nano-diodes depends critically on the characteristics of their constituent materials (principally the metal work function and semiconductor Femi level) as well as the specifics of the device geometry. There is a significant interplay in how these factors affect the generation of hot electrons, and the probability for the contribution of the generated hot electrons to the photocurrent. We may define external quantum efficiency (EQE) as the ratio of the number of hot electrons emitted tunneling through the barrier divided by the number of photons incident on the nanohole, as:

$$\mathrm{EQE} = \frac{hc}{e\lambda}\mathrm{R}(\lambda) \qquad (2)$$

Where $\boldsymbol{h}$ is Planck constant, $\boldsymbol{c}$ is the velocity of light in vacuum, $\boldsymbol{e}$ is the electron charge and $\boldsymbol{\lambda}$ is the wavelength of the incident laser. The spectral responsivity, $\mathbf{R}(\boldsymbol{\lambda}) = \Delta \boldsymbol{I}/\boldsymbol{P}_{\boldsymbol{optical}}$, is the ratio of the response current to the incident monochromatic optical power (the responsive photocurrent and the laser power incident on the device are denoted by $\Delta \boldsymbol{I}$ and $\boldsymbol{P}_{\boldsymbol{optical}}$, respectively). Table 1 compares this present study with the other reported similar structures. All, previously reported high EQE values to date have been obtained at short wavelengths. Here, based on our empirical findings, we calculate an EQE of ~4% at different laser powers (Figure 3d), which was achieved at long wavelength (λ =800 nm), several orders of magnitude higher than other similar devices.

Table 1. Comparison of typical plasmonic hot electron nanoscale diode performance parameters.

Structure	Materials	Excitation wavelength	EQE	Reference
MIS structure	FTO-TiO_2-Al_2O_3-Ag	460 nm	4%	[25]
MIS structure	FTO-TiO_2-Al_2O_3-Au	550 nm	1.3%	[25]
MIM structure	Ag-polymer-Ag	680 nm	0.18%	[26]
MIS structure	Au-SiO_2-Si	720 nm	0.01% (IQE)	[27]
Lateral tunnel junction	Au	730-780 nm	0.03%	[28]
MIS structure	Au-SiO_2-Si	800 nm	4%	Our work
Nanowire array	Au/Ti-SiO_2	1200-1800 nm	0.05-0.1% (IQE)	[29]
Nanorods array	ITO-SiO_2-Au	1250-1600 nm	0.01% (IQE)	[10]
Nano grating structure	Au-Si	1295-1635 nm	0.2% (IQE)	[30]

Conclusions

Here we have demonstrated photoelectron generation by hot electron formation in vacuum channel nano-diodes. The voltage-dependence, temperature-dependence, laser power-dependence, polarization-dependence and spectra-dependence of the photocurrent have been experimentally determined. The EQE of the vacuum channel nano-diodes was ~4%, several orders of magnitude higher than other similar devices. Moreover, the absorption peak of the photoresponse current have been corroborated by theoretical calculations and experimental verification. By utilizing arrays of nano-diodes as direct light collection and carrier generation elements, both polarization and wavelength selective detectors can be implemented without the need for additional optical components. The investigated device has shown impressive functionality as a high-efficiency light modulation detector in weak light environments. With a diverse range of potential applications, the present nano MIS structures offer a new method of mediating light-matter interactions, creating additional and unpredictable applications in the fields of light-sensing, energy conversion and miniaturized photodetection technologies.

Experimental section

Fabrication Process of Vacuum Channel Nanoscale Diode

The vacuum channel nano-diodes were fabricated by performing FIB etching on a silicon MIS substrate. A 30-nm-thick SiO_2 layer was first grown by atomic layer deposition (ALD, SI-ALD) on n-type silicon (phosphorus-doped, resistivity = 0.003 Ω cm) wafers ((100)-oriented; thickness, 500±10 μm). A gold electrode (thickness, 60 nm) was prepared on the top of the insulator layer by electron beam evaporation in conjunction with an electron beam lithography and lift-off process. After the formation of the MIS structure, the MIS wafers were further processed to develop nanoscale-void vertical channels using a FIB etching technique. The FIB etching process was performed with a FIB/SEM Dual Beam System (FEI-Nova200). A gallium ion beam (30 keV, 10 pA) was used with a dwell time of 39 s to create rectangular nanoholes arrays (cross-sections, 500 nm × 100 nm) in silicon MIS wafers (Figure 1b).

Characterization and Electronic Measurements

The morphologies of the vacuum channel nano-diodes were characterized by SEM (FEI NOVA Nano-430). The I-V characteristics of the vacuum channel nano-diodes were measured in the dark with a semiconductor parameter analyzer (Keithley Model 4200-SCS). Incident light from a supercontinuum laser source (Wuhan YSL Photonics, SC-Pro7) was focused on the sample using 10× Olympus objective (MplanFL, NA = 0.50) and the photoresponse was measured using a Keithley sourcemeter 2636B. The optical images were obtained by the same objective, and recorded using a CCD camera (DVC company, 710M-00-FW) to confirm the laser position on the nanoholes.

Simulations

The optical absorption spectra and the electromagnetic field distribution of the vacuum channel nanoscale diodes were simulated by using the finite element method. The parameters taken in the simulation correspond to the experiment.

Conflicts of interest

There are no conflicts to declare.

Acknowledgements

This work was supported by the National Key R&D Program of China (Grant No. 2016YFA0202001), and the National Natural Science Foundation of China (Grant Nos. 11427808 and 51602071).

References

1. M. F. A. S. Obayya, M.F.O Hameed, M. Hussein, *Optical nano-antennas for energy harvesting*, IGI Global, 2015.
2. E. Briones, J. Alda and F. Javier Gonzalez, *Optics Express*, 2013, **21**, A412-A418.

3. G. A. E. Vandenbosch and Z. Ma, *Nano Energy*, 2012, **1**, 494-502.
4. M. Dagenais, K. Choi, F. Yesilkoy, A. N. Chryssis and M. C. Peckerar, in *Optoelectronic Integrated Circuits Xii*, eds. L. A. Eldada and E. H. Lee, 2010, vol. 7605.
5. R. L. Olmon, P. M. Krenz, A. C. Jones, G. D. Boreman and M. B. Raschke, *Optics Express*, 2008, **16**, 20295-20305.
6. C. Hoppener and L. Novotny, *Nano Letters*, 2008, **8**, 642-646.
7. A. Weber-Bargioni, A. Schwartzberg, M. Cornaglia, A. Ismach, J. J. Urban, Y. Pang, R. Gordon, J. Bokor, M. B. Salmeron, D. F. Ogletree, P. Ashby, S. Cabrini and P. J. Schuck, *Nano Letters*, 2011, **11**, 1201-1207.
8. W. Li, Z. J. Coppens, L. V. Besteiro, W. Wang, A. O. Govorov and J. Valentine, *Nature Communications*, 2015, **6**.
9. L. Novotny and N. van Hulst, *Nature Photonics*, 2011, **5**, 83-90.
10. M. W. Knight, H. Sobhani, P. Nordlander and N. J. Halas, *Science*, 2011, **332**, 702-704.
11. W. P. Putnam, R. G. Hobbs, P. D. Keathley, K. K. Berggren and F. X. Kaertner, *Nature Physics*, 2017, **13**, 335-339.
12. T. Rybka, M. Ludwig, M. F. Schmalz, V. Knittel, D. Brida and A. Leitenstorfer, *Nature Photonics*, 2016, **10**, 667-670.
13. T. Ando, A. B. Fowler and F. Stern, *Reviews of Modern Physics*, 1982, **54**, 437-672.
14. A. Toriumi, M. Yoshimi, M. Iwase, K. Taniguchi and C. Hamaguchi, *Surface Science*, 1986, **170**, 363-369.
15. S. Han and J. Ihm, *Physical Review B*, 2000, **61**, 9986-9989.
16. X. Zheng, G. H. Chen, Z. B. Li, S. Z. Deng and N. S. Xu, *Physical review letters*, 2004, **92**.
17. A. Mayer, *Physical Review B*, 2005, **71**.
18. S. Srisonphan, Y. S. Jung and H. K. Kim, *Nat Nanotechnol*, 2012, **7**, 504-508.
19. H. Chalabi, D. Schoen and M. L. Brongersma, *Nano Lett*, 2014, **14**, 1374-1380.
20. J. Hofmann and Steinman.W, *Physica Status Solidi*, 1968, **30**, K53-&.
21. J. G. Endriz and W. E. Spicer, *Physical Review Letters*, 1970, **24**, 64-&.
22. T. Inagaki, K. Kagami and E. T. Arakawa, *Physical Review B*, 1981, **24**, 3644-3646.
23. T. Inagaki, K. Kagami and E. T. Arakawa, *Applied Optics*, 1982, **21**, 949-954.
24. J. Lehmann, M. Merschdorf, W. Pfeiffer, A. Thon, S. Voll and G. Gerber, *Physical Review Letters*, 2000, **85**, 2921-2924.
25. F. P. G. de Arquer, A. Mihi, D. Kufer and G. Konstantatos, *ACS Nano*, 2013, **7**, 3581-3588.
26. H. Qian, S.-W. Hsu, K. Gurunatha, C. T. Riley, J. Zhao, D. Lu, A. R. Tao and Z. Liu, *Nature Photonics*, 2018, **12**, 485-+.
27. H. Goktas, F. S. Gokhan and V. J. Sorger, *Acs Photonics*, 2018, **5**, 4928-4936.
28. J. Kern, R. Kullock, J. Prangsma, M. Emmerling, M. Kamp and B. Hecht, *Nature Photonics*, 2015, **9**, 582-+.
29. M. W. Knight, Y. Wang, A. S. Urban, A. Sobhani, B. Y. Zheng, P. Nordlander and N. J. Halas, *Nano Letters*, 2013, **13**, 1687-1692.
30. A. Sobhani, M. W. Knight, Y. Wang, B. Zheng, N. S. King, L. V. Brown, Z. Fang, P. Nordlander and N. J. Halas, *Nature Communications*, 2013, **4**.